**Structural Engineering and Mechanics**, *Vol. 57, No. 2 (2016) 281-294*
DOI: http://dx.doi.org/10.12989/sem.2016.57.2.281 

# A mesh-free analysis method of structural elements of engineering structures based on B-spline wavelet basis function

Jianping Chen[*1,2], Wenyong Tang[2a], Pengju Huang[1] and Li Xu[3]

[1]*School of Ship Engineering, Guangzhou Maritime Institute, Guangzhou, China*
[2]*School of Naval Architecture, Ocean & Civil Engineering, Shanghai Jiao Tong University, Shanghai, China*
[3]*Fujian Chuanzheng Communications College, Fuzhou, China*

*(Received January 20, 2015, Revised November 3, 2015, Accepted December 18, 2015)*

**Abstract.** The paper is devoted to study a mesh-free analysis method of structural elements of engineering structures based on B-spline Wavelet Basis Function. First, by employing the moving-least square method and the weighted residual method to solve the structural displacement field, the control equations and the stiffness equations are obtained. And then constructs the displacement field of the structure by using the *m*-order B-spline wavelet basis function as a weight function. In the end, the paper selects the plane beam structure and the structure with opening hole to carry out numerical analysis of deformation and stress. The Finite Element Method calculation results are compared with the results of the method proposed, and the calculation results of the relative error norm is compared with Gauss weight function as weight function. Therefore, the clarification verified the validity and accuracy of the proposed method.

**Keywords:** structural analysis; moving-least square method; meshless local MLPG method; B-Spline wavelet weight function

## 1. Introduction

Currently, the Finite Element Method (hereafter abbreviated as FEM) is one of most important tools in numerical analysis. FEMs have been widely applied to assess, process and simulate the structural deformation, stress and fatigue and so on (Cui *et al.* 1998, Na and Karr 2013, Norwood and Dow 2013, Senjanovic *et al.* 2013). However, FEM has some disadvantages because of its own characteristics. Its calculation is not accurate enough and sometimes even interrupted while processing the displacement and stress fields in high-gradient regions. In order to solve this problem, FEMs adopt the method of refining the mesh (subdivision) or employ higher-order unit in the problem domain, which requires FEMs to be strong adaptive approach. Consequently, the pre-processing and post-processing works will increase and relatively the computational efficiency will rapidly reduce. In fact, FEMs can't absolutely eliminate the previous problems arising from

*Corresponding author, Ph.D., E-mail: wchchenjp@sina.com
[a]Professor, E-mail: wytang@sjtu.edu.cn


http://www.techno-press.org/?journal=sem&subpage=8 ISSN: 1225-4568 (Print), 1598-6217 (Online)

the structural deformation and stress in high-gradient regions.

As an alternative numerical analysis method to FEMs, the mesh-free (mesh-less or element-free) methods have been attracting much more attention (Tezduyar 2003, Belytschko *et al.* 1996, Liu *et al.* 1999, Atluri and Shen 2005, Oden *et al.* 1998) since two decades ago. Based on constructing a serial of discretization nodes, mesh-free method solves the problems by constructing the field approximation function. Compared with conventional finite element methods, the mesh-free methods don't need any meshing background. It is easy for us to increase or decrease nodes without any additional dealing with topology information between nodes in the course of calculation. Therefore the mesh-free method is particularly suitable for adaptive analysis and calculation. Moreover, it is unnecessary to create mesh for the structures. Thus it can save time and computing resources in generating and processing mesh. Mesh-free methods are widely involved in many fields (Liu and Gu 2000, He *et al.* 2006, Duan and Wang 2013, Johnson *et al.* 2002), such as moving boundary problem, aviation materials, high-speed collision, dynamic crack propagation, molding, jointed rock analyzes, etc.

Actually, the calculation accuracy of mesh-free method is impacted by its own characteristics, such as the density of nodes, the kind of basis function, its order and the scale of supporting domain and so on. It is paramount how to select the basis function and decide the scale of the support domain to solve the problem (Liu 2003). In addition, the scale of influence domain (support domain) is eventually determined by the fitting weight function. It is therefore vital to select a suitable weight function for approximate solutions and real solutions of approximation degree (Atluri and Zhu 1998). The paper presents a mesh-free analysis method that employs B-spline wavelet weight function to assess the membrane (in-plane) structures according to above situation mentioned. Chen *et al*. (2015) presented a mesh-free analysis of the Ship Structures Based on Daubechies Wavelet Basis theory. This thesis by Chen *et al*. (2015) directly used DB wavelet analysis structure to construct the approximation function of the field, while the B-spline wavelet was regarded as a weight function in MLS employed in this thesis. Based on meshless local Petrov-Galerkin method, the paper employs m-order B-Spline wavelet basis function as the weight function. Numerical illustrative examples verified the validity of the proposed MLPG for the structures analysis.

## 2. System equations of structural elements by MLPG

In ship structure analysis, the thin plate structure is often simplified as a membrane structure in order to simplify the analysis. In this section, the meshless local Petrov-Galerkin method (MLPG) is applied to analyze the membrane.

### *2.1 Governing equation*

For the discretized plane structure, its system equations are given on the basis of two-dimensional elastic theory

$$\boldsymbol{\sigma}_{ij,i} + \mathbf{b}_i = \mathbf{0}\,, \tag{1}$$

Where $i$ and $j$ are relatively the two directions of the 2-dimensional plane. $\boldsymbol{\sigma}_{ij,i}$ denotes the stress component along the $i$ direction, and $\mathbf{b}_i$ is the body force component in the $i$ direction.

$\boldsymbol{\Omega}$ is defined as the problem domain, and $\boldsymbol{\Gamma}$ is defined as the boundary of $\boldsymbol{\Omega}$.

The essential boundary condition is $\mathbf{u}_i = \bar{\mathbf{u}}_i$, and $\mathbf{\Gamma}_\mathbf{u}$ is the essential boundary.

The natural boundary condition is $\boldsymbol{\sigma}_{ij}\mathbf{n}_i = \bar{\mathbf{t}}_i$, $\mathbf{\Gamma}_\mathrm{t}$ is the natural boundary, and $\mathbf{n}_i$ is the $j$-th component of unit outward normal vector of the natural boundary condition.

By employing the weighted residual method (Johnson *et al*. 2002), the strong form of differential equations of the system equations with respect to Node $I$ can be obtained as following

$$\int_{\Omega_Q} (\boldsymbol{\sigma}_{ij,i} + \mathbf{b}_i)\hat{W}_I d\mathbf{\Omega} - \alpha \int_{\Gamma_{Q_u}} (\mathbf{u}_i - \bar{\mathbf{u}}_i)\hat{W}_I d\mathbf{\Gamma} = 0 \tag{2}$$

Where $\hat{W}$ is a weight function, $\mathbf{\Omega}_Q$ is the integration domain of the node $I$, $\mathbf{\Gamma}_Q$ is the its boundary and $\alpha$ is a penalty factor. In addition, $\mathbf{\Gamma}_{Q_u}$ is the overlap of the integration domain $\mathbf{\Omega}_Q$ and the essential boundary $\mathbf{\Gamma}_u$.

According to Eq. (2), for the $I$ node, its system equation can be established while integrating in its integration domain. Thereby, the system equation of each node can be obtained in its integration domain by employing Eq. (2). And the system equations can be obtained for all of the discrete nodes. Assembling these system equations, the overall system equations of the problem domain are established.

For each node, the shape function is obtained by moving-least squares method (MLS) in its supporting integration domain, and the approximation function of displacement field is obtained in the problem domain (Zienkiewicz 1989).

$$u^h(\mathbf{X}) = \mathbf{\Phi}^T(\mathbf{X}) \cdot \mathbf{u} = \sum_{I=1}^{N} \phi_I(\mathbf{X}) u_I \tag{3}$$

In which $\mathbf{\Phi}^T(\mathbf{x})$ is the matrix of shape function connecting the approximation function of the node according to MLS. $u_I$ is the parameter value of the discrete node $I$. $N$ is the number of the node in the supporting domain $\mathbf{\Omega}_s$ of the integration point.

According to elastic stress-strain relations, there is

$$\boldsymbol{\sigma} = \mathbf{D}\boldsymbol{\varepsilon} = \mathbf{D}\mathbf{L}\mathbf{u}^h = \mathbf{D}\begin{bmatrix} \dfrac{\partial}{\partial x} & 0 \\ 0 & \dfrac{\partial}{\partial y} \\ \dfrac{\partial}{\partial y} & \dfrac{\partial}{\partial x} \end{bmatrix} \sum_j^n \mathbf{\Phi}_j \mathbf{u}_j = \mathbf{D}\sum_j^n \mathbf{B}_j \mathbf{u}_j \tag{4}$$

Where $\mathbf{D}$ is the plane-stress constitutive matrix, $\mathbf{B}$ is the strain-displacement matrix, and $\mathbf{B}_j$ is defined as follows,

$$\mathbf{B}_j = \begin{bmatrix} \phi_{j,x} & 0 \\ 0 & \phi_{j,y} \\ \phi_{j,y} & \phi_{i,x} \end{bmatrix}.$$

Supposed $\hat{V}_I$ is the Jacobian matrix of the weighted function $\hat{W}_I$, Eq. (2) can be derived as following

$$\int_{\Omega_Q} \hat{\mathbf{V}}_I \boldsymbol{\sigma} d\boldsymbol{\Omega} + \alpha \int_{\Gamma_{Qu}} \hat{\mathbf{W}}_I \mathbf{u} d\boldsymbol{\Gamma} - \int_{\Gamma_{Qu}} \hat{\mathbf{W}}_I \mathbf{N} \boldsymbol{\sigma} \mathbf{d}$$
$$= \int_{\Gamma_{Qt}} \hat{\mathbf{W}}_I \bar{\mathbf{t}} d\boldsymbol{\Gamma} + \alpha \int_{\Gamma_u} \hat{\mathbf{W}}_I \bar{\mathbf{u}} d\boldsymbol{\Gamma} + \int_{\Omega_Q} \hat{\mathbf{W}}_I \mathbf{b} d\boldsymbol{\Omega} \quad (5)$$

Where $\boldsymbol{\Gamma}_{Q_t}$ is the overlapping part of the integration domain $\boldsymbol{\Omega}_Q$ and the natural boundary. **N** is the unit outward normal matrix of the natural boundary.

### *2.2 Stiffness matrix*

For Node *I*, substituting the node system equation Eq. (3) and Eq. (4) into the governing equation Eq. (5), it can be shown as

$$\int_{\Omega_Q} \hat{\mathbf{V}}_I^T \sum_j^n \mathbf{B}_j \mathbf{u}_j d\boldsymbol{\Omega} + \alpha \int_{\Gamma_{Qu}} \hat{\mathbf{W}}_I \sum_j^n \boldsymbol{\Phi}_j \mathbf{u}_j d\boldsymbol{\Omega} - \int_{\Gamma_{Qu}} \hat{\mathbf{W}}_I \mathbf{N} \sum_j^n \mathbf{B}_j \mathbf{u}_j d\boldsymbol{\Gamma}$$
$$= \int_{\Gamma_{Qt}} \hat{\mathbf{W}}_I \bar{\mathbf{t}} d\boldsymbol{\Gamma} + \alpha \int_{\Gamma_{Qu}} \hat{\mathbf{W}}_I \bar{\mathbf{u}} d\boldsymbol{\Gamma} + \int_{\Omega_Q} \hat{\mathbf{W}}_I \mathbf{b} d\boldsymbol{\Omega} \quad (6)$$

Eq. (6) can be shortened as the following matrix form

$$\mathbf{K}_I \mathbf{u} = \mathbf{F}_I , \quad (7)$$

Where

$$\mathbf{K}_I = \sum_j^n \mathbf{K}_{Ij} = \int_{\Omega_Q} \hat{\mathbf{V}}_I^T \sum_j^n \mathbf{B}_j d\boldsymbol{\Omega} + \alpha \int_{\Gamma_{Qu}} \hat{\mathbf{W}}_I \sum_j^n \boldsymbol{\Phi}_j d\boldsymbol{\Omega} - \int_{\Gamma_{Qu}} \hat{\mathbf{W}}_I \mathbf{N} \sum_j^n \mathbf{B}_j d\boldsymbol{\Gamma} ,$$

and $\mathbf{F}_I = \int_{\Gamma_{Qt}} \hat{\mathbf{W}}_I \bar{\mathbf{t}} d\boldsymbol{\Gamma} + \alpha \int_{\Gamma_{Qu}} \hat{\mathbf{W}}_I \bar{\mathbf{u}} d\boldsymbol{\Gamma} + \int_{\Omega_Q} \hat{\mathbf{W}}_I \mathbf{b} d\boldsymbol{\Omega}$.

By assembling these nodes discrete system equations, the overall system governing equations of the problem domain can be expressed as

$$\mathbf{K}\mathbf{u} = \mathbf{F} . \quad (8)$$

In MLS technique, the supporting domain of the node is compactly supported. Therefore, the overall stiffness matrix **K** is the banded sparse matrix. Taking such a matrix form, can greatly reduce the amount of computation.

## 3. B-spline wavelet basis function

In MLPG method, employing the moving least squares method (MLS) is the key to solve the approximating function of the displacement field. In mesh-free method, the weight function is required as a compactly supporting function, and it is consecutive and differentiable, monotone decreasing and normal compactly in solving domain and so on (Yang and Li 2005). The wavelet function has variable scale capacity, which can express the function at different resolution levels. Wavelet function's corresponding basis function (wavelet basis) not only has shock, attenuation but also compact supporting or approximate compact supporting (Long and Hu 2003, Mallat

1989).That is to say, B-spline function is segmentation smooth, local differentiable and linear combination (Qin 2012).

Therefore, the B-spline wavelet function with time frequency local characteristic is the most similar Gauss function as the weight function among mesh-free method. Also its compact supporting nature is superior to Gauss function. This advantage has guaranteed its phase will not be distortion in the course of processing computation. The paper constructs the wavelet basis function as the weight function for MLPG method by combining the respective advantage of wavelet function and B-spline function.

For the *m*-order B-spline function space, it is constructed of the spline functions from the sequence of the nodes serial $\left\{x_k^j\right\}_{k=-m+1}^{2^j+2m-1}$ ( the total amount of the nodes is $2^j$+2*m*−1, and the sequence of the node serial $\left\{x_k^j\right\}_{k=-m+1}^{2^j+2m-1}$ are defined by the reference (Yang and LI 2005)

$$\begin{cases} x_{-m+1}^j = x_{-m+2}^j = \cdots = 0 \\ x_k^j = k2^j, k = 1, 2^1, \cdots, 2^j \\ x_{2^j+1}^j = x_{2^j+2}^j = \cdots = x_{2^j+m-1}^j = 1 \end{cases} \tag{9}$$

According to Eq. (9), the *j*-th scaling approximation space $V_J^{[0,1]}$ of the *m*-order local supporting nesting can be inferred in interval [0,1], and its basis function is expressed as

$$\begin{cases} B_{m,k}^j(x) = N_m\left(2^j\xi - k\right),\ k = -m+1, -m+2, \cdots, 2^j - 1 \\ \sup pB_{m,k}^j = \left[\xi_k^j, \xi_{k+m}^j\right] \end{cases} \tag{10}$$

Where $N_m(x)$ is the basis spline function.

In the restricted interval [0,1], if the wavelet scaling function $\varphi_{m,k}^j(\xi) = B_{m,k}^j(\xi)$ is satisfied, the condition $2^j \geq 2m-1$ should be satisfied. So the *m*-order B-spline scaling function $\phi_{m,k}^j(\xi)$ for any scaling *j* can be inferred as following (Cui and Quak 1993)

$$\phi_{m,k}^j(\xi) = \begin{cases} \phi_{m,k}^l\left(2^{j-l}\xi\right), k = -m+1, -m+2, \cdots, -1 \\ \phi_{m,2^j-m-k}^l\left(1-2^{j-l}\xi\right), k = 2^j - m + 1, \cdots, 2^j - 1 \\ \phi_{m,0}^l\left(2^{j-l}\xi - 2^{-l}k\right), k = 0, 1, \cdots, 2^j - m \end{cases} \tag{11}$$

The wavelet function $\phi_{m,k}^j(\xi)$ corresponding to $\varphi_{m,k}^j(\xi)$ can be written as

$$\varphi_{m,k}^j(\xi) = \begin{cases} \phi_{m,k}^l\left(2^{j-1}\xi\right), k = -m+1, -m+2, \cdots, -1 \\ \phi_{m,2^j-m-k}^l\left(1-2^{j-l}\xi\right), k = 2^j - 2m - 2, \cdots, 2^j - m \\ \phi_{m,0}^l\left(2^{j-l}\xi - 2^{-l}k\right), k = 0, 1, \cdots, 2^j - 2m + 1 \end{cases} \tag{12}$$

The wavelet compactly supporting space in local field can be expressed as

$$\sup p\varphi_{m,k}^{j}(\xi)=\begin{cases}\left[k2^{-j},(2m-1+k)2^{-j}\right]\\ \left[0,(2m-1+k)2^{-j}\right]\\ \left[k2^{-j},1\right]\end{cases} \tag{13}$$

The paper selects 3-order B-spline wavelet function, namely $m$=3. The basis expression formulation of 3-order B-spline wavelet function can be written as

$$\varphi(x)=\frac{1}{6}\begin{cases}(x+2)^3 & x\in[-2,-1]\\ (x+2)^3-4(x+1)^3 & x\in[-1,0]\\ (2-x)^3-4(1-x)^3 & x\in[0,1]\\ (2-x)^3 & x\in[1,2]\\ 0 & |x|\geq 2\end{cases} \tag{14}$$

Because the selection of the weight function directly affects the accuracy of the meshless method, it is supposed to be matched in the selection process. In order to make 3-order B-spline wavelet meet the selection principle, according to the characteristics of the wavelet function, Eq. (14) can be made the transformation as,

$$\varphi(x)=\frac{1}{6}\begin{cases}\left[(x-a)/b+2\right]^3 & x\in[-2,-1)\\ \left[(x-a)/b+2\right]^3-4\left[(x-a)/b+1\right]^3 & x\in[-1,0)\\ \left[2-(x-a)/b\right]^3-4\left[1-(x-a)/b\right]^3 & x\in[0,1)\\ \left[2-(x-a)/b\right]^3 & x\in[1,2)\\ 0 & x\geq 2\end{cases} \tag{15}$$

Where, $a$,$b$ are constant. In general, the value range of $a$ is (−1,1), and the value range of $b$ is (1,2). Their specific value need to be adjusted as per the accuracy of the requirements to make approximation analytical solution.

## 4. Essential boundary conditions

Due to the meshless shape function $\mathbf{\Phi}^T(\mathbf{x})$ not satisfying the Kronecker delta condition, the parameter of node $I$ is not the true displacement in the stiffness equation Eq. (7), so the essential boundary conditions can't be directly applied like the finite element method. Chen *et al*. (1996) introduced the Full transformation method to enforce the essential boundary conditions. The stiffness equations are re-corrected in accordance with the Full transformation method. The basic principle of the Full transformation method is described as following.

Considering approximate displacement is

$$u^h(x)=\sum_{I=1}^{N}\phi_I(x)u_I \tag{16}$$

The true displacement is

$$\bar{u} \approx u^h(x) = \sum_{I=1}^{N} \phi_I(x) u_I = \mathbf{\Phi u} \tag{17}$$

Where $\mathbf{\Phi} = \begin{bmatrix} \phi_1(x_1) & \phi_2(x_1) & \cdots & \phi_n(x_1) \\ \phi_1(x_2) & \phi_2(x_2) & \cdots & \phi_n(x_2) \\ \vdots & \vdots & \ddots & \vdots \\ \phi_1(x_n) & \phi_2(x_n) & \cdots & \phi_n(x_n) \end{bmatrix}$

So there is

$$\mathbf{u} = \mathbf{\Lambda}\bar{\mathbf{u}} \tag{18}$$

Where $\mathbf{\Lambda}=\mathbf{\Phi}^{-1}$

The system governing equations are expressed as

$$\mathbf{ku} = \mathbf{F} \Rightarrow \mathbf{\Lambda}^{\mathrm{T}}\mathbf{K}\mathbf{\Lambda}\bar{\mathbf{u}} = \mathbf{\Lambda}^{\mathrm{T}}\mathbf{F}\mathbf{\Lambda} \tag{19}$$

Denoting $\mathbf{K}=\mathbf{\Lambda}^{\mathrm{T}}\mathbf{T}\mathbf{K}\mathbf{\Lambda}$ and $\bar{\mathbf{F}} = \mathbf{\Lambda}^{\mathrm{T}}\mathbf{F}\mathbf{\Lambda}$ , for node *I*, Eq. (8) can be re-written as

$$\bar{\mathbf{K}}_I \bar{\mathbf{u}} = \bar{\mathbf{F}}_I \tag{20}$$

## 5. Numerical examples

In order to verify the validity of the proposed method of the paper, there are two numerical illustrative examples, one is the plane beam structure with openings, and the other one is the structure with opening hole. In following examples, the Young's modulus is $E$=2.1×10$^5$ MPa, and Poisson's ratio is $\mu$=0.3.

In the paper, the structure is discretized by the method of automatic discretization, and the generation of the initial node is randomly distributed, and it is not uniform. While calculating the parameters of each discrete node and the approximate field function, the paper presented method employing 3-order B-spline wavelet as the weight function, and the influence domains of the weight function are taken as the supporting domains of the nodes.

In the presented method, the rectangular domain is taken as the influenced domain of the B-spline wavelet weight function and the influence domain of the B spline wavelet power function in the moving-least square method. The length of the rectangular region is defined as following

$$\begin{cases} r_q = \alpha d_e \\ r_i = \beta d_e \end{cases} \tag{21}$$

Where $r_q$ is the length of integration domain, $r_i$ is the length of influence domain, and $d_e$ is the shortest distance among nodes. $\alpha$ is the length coefficient of integration domain, and it is taken 1.5. $\beta$ is the length coefficient of influence domain, and it is taken 3.0. Integration domain is subdivided into 2×2 integration grids, and each grid takes 3×3 Gauss integration points.

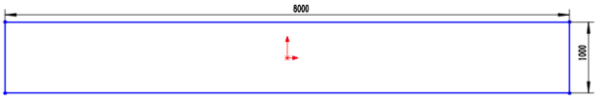


Fig. 1 Typical beam structure under uniform pressure

(a) Mesh-free discretized node figure (b) ANSYS meshing figure

Fig. 2 Arrangement of the node with Mesh-free and FEM

(a) Mises-stress cloud figure with MLPG (b) Mises-stress cloud figure with ANSYS

Fig. 3 Mises-stress cloud figure with MLPG and FEM

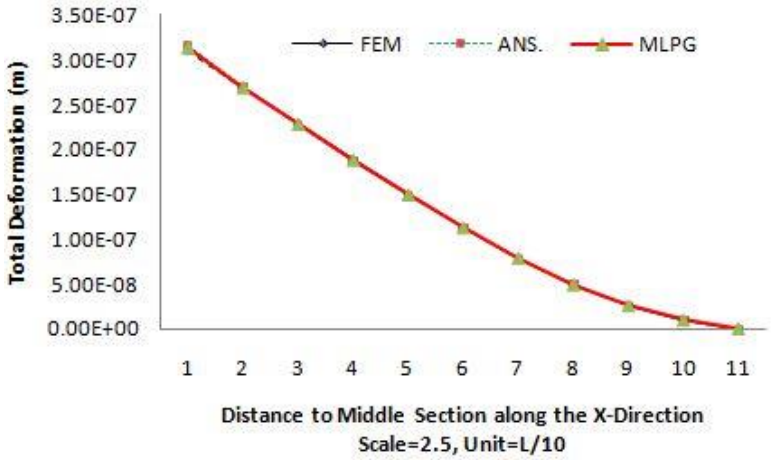


Fig. 4 Total deformation of the middle section along the *X*-direction

### *5.1 Beam structure*

Simplifying the ship beam structure as shown in Fig. 1, one side is fixed, and the other side is free. The top edge is subjected to a uniform pressure $p$=10 N/m.

Fig. 2(a) is a discretized node figure through a four-step adaptive algorithm employing the proposed mesh-free method. The initial distributed nodes are 90 points, and the integral background meshes are 351 points. After a four-step adaptive analysis, the number of nodes reaches to 387, the integral background meshes are 1210. Fig. 2(b) is the meshing map employing ANSYS (FEM).

The mises-stress map is shown as Fig. 3(a) with the presented MLPG. Comparing with the calculation result of the finite element software ANSYS, which the stress map is shown as Fig. 3(b), the stress concentration regions are consistent.

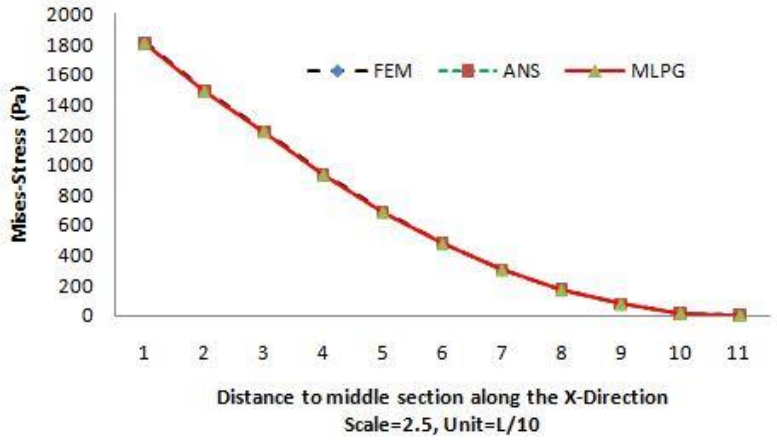


Fig. 5 Mises-stress of the middle section along the *X*-direction

For simplicity, only the total deformation of middle section along the *X*-direction and mises-stress of middle section along the *X*-direction are compared between the proposed method and FEMs (ANSYS), as shown in Fig. 4 and Fig. 5 under the wavelet basis *Scale*=2.5. (In the figure, FEM means the solution of the FEM, ANS denotes the analytical solution, and MLPG denotes the solution with the proposed method). There are two conclusions from the compared figure: First, FEM and MLPG computation relative error norm all are below 5%. Secondly, the proposed method is closer analytic solution compared to FEM method. Obviously, this paper proposed method has very high computation accuracy.

In order to further analyze the correctness and precision of the method, under the condition of selecting the same scale parameter, there shows the relative error norm of the displacement and stress with Gauss weight function, and compares them with the proposed method.

The relative error norm of the displacement $L_u$ is defined by

$$L_u = \sqrt{\sum_I^N \left[u(x_I) - u^h(x_I)\right]^2} \Big/ \sum_I^N u^2(x_I) \tag{22}$$

The relative error norm of the stress $L_\sigma$ is defined by

$$L_\sigma = \sqrt{\sum_I^N \left[\sigma(x_I) - \sigma^h(x_I)\right]^2} \Big/ \sum_I^N \sigma^2(x_I) \tag{23}$$

The results of calculation are shown as Table 1.

Table 1 shows as the relative error norm with the proposed method under various scales, and it is described with the error curve as Fig. 6. From Table 1 and Fig. 6, conclusion can be drawn that computation accuracy is affected by the scale parameter. When 3-order B-spline wavelet function is used as a weight function, the results are better than Gauss weight function as weight function.

Table 1 The relative error norm with 3-order B-spline wavelet and Gauss weight function

| Scale | 2 | 2.1 | 2.5 | 2.8 | 3 | 3.5 | 4 |
|---|---|---|---|---|---|---|---|
| $L_u$-B | 4.7734 | 3.4507 | 0.6516 | 3.3632 | 3.4613 | 1.5705 | 2.3853 |
| $L_\sigma$-B | 4.9048 | 3.4261 | 1.3118 | 3.3479 | 3.4579 | 1.6858 | 2.347 |
| $L_u$-G | 12.6074 | 15.568 | 7.1611 | 1.0792 | 5.5468 | 9.7283 | 4.7734 |
| $L_\sigma$-G | 13.0931 | 15.6777 | 7.2242 | 2.1391 | 6.0378 | 9.7422 | 4.9048 |

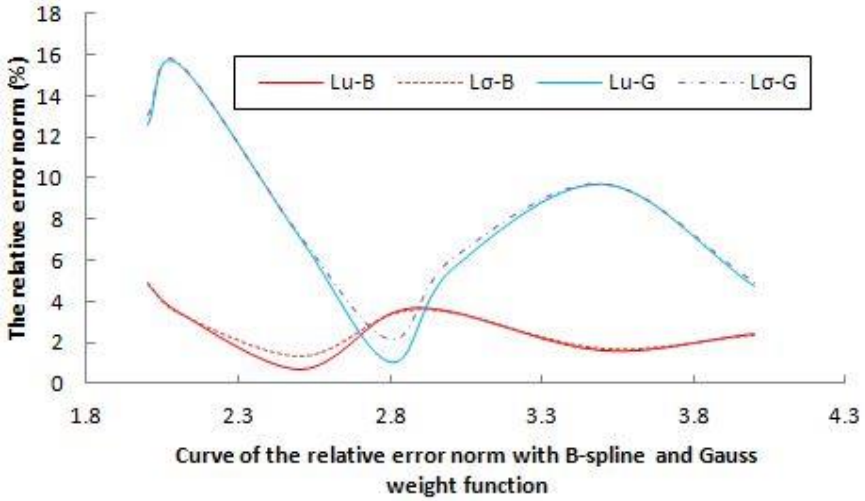


Fig. 6 The relative error norm with 3-order B-spline wavelet and Gauss weight function

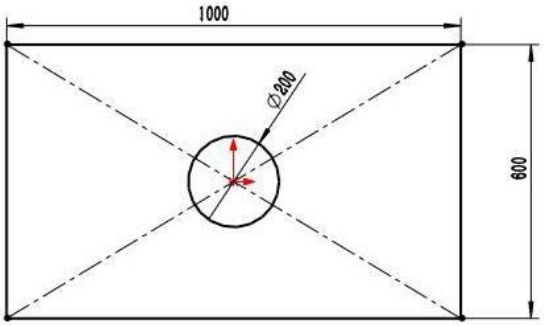


Fig.7 The plate with a circular opening

In addition, the proposed method can achieve a good accuracy in the case of small support domain, namely, while *Scale*=2.5, it can achieve a higher fitting.

### *5.2 Structure with opening hole*

Simplifying the structure as the flat plate as Fig. 7 shown, the two edges are free, and the other two edges are subjected to a uniform tension $q$=1 MPa. The plate has a circular opening hole in the center.

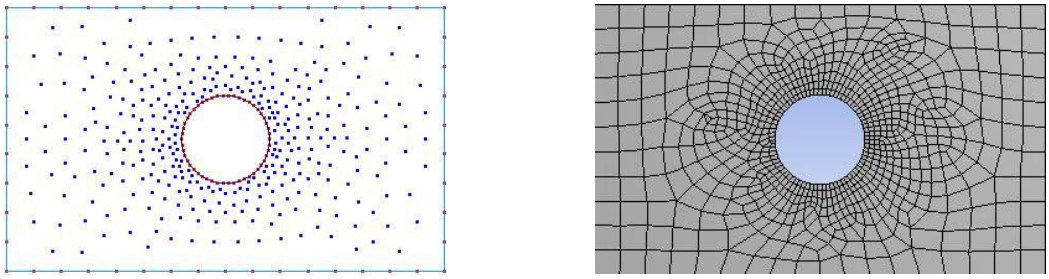

(a) Mesh-free discrete node graph (b) ANSYS meshing graph

Fig. 8 Arrangement of the node with Mesh-free and FEM

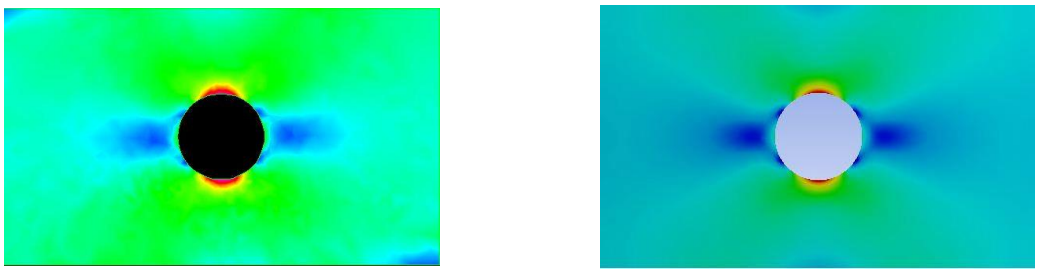

(a) Mises-stress cloud figure with MLPG (b) Mises-stress cloud figure with ANSYS

Fig. 9 The Mises-stress map with MLPG and FEM

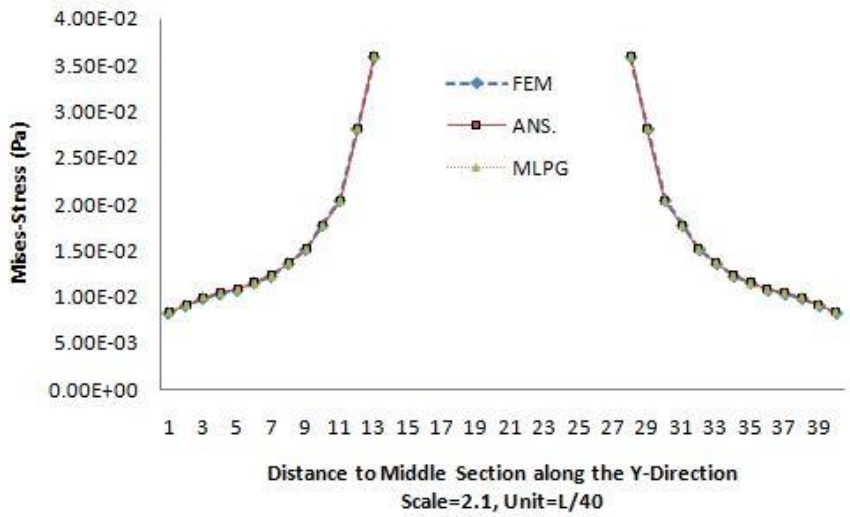


Fig.10 Mises-stress of the middle section along the *Y*-direction

Fig. 8(a) is a discrete node figure through a four-step adaptive algorithm employing the proposal mesh-free methods. The initial evenly distributed nodes are 379 nodes, the integral background meshes are 1390 points, after a four-step adaptive analysis, the number of nodes reach to 1323, the integral background meshes are 2515. Fig. 8(b) is the meshing map employing ANSYS (finite element method).

The mises-stress map is shown as Fig. 9(a) with the presented MLPG. Comparing with the calculation result of the finite element software ANSYS, which the stress map is shown as Fig. 9(b), the stress concentration regions are consistent.

Further comparison with the results of the finite element method (ANSYS), for simplicity, only compares the total deformation of middle section along the *X*-direction and mises-stress of middle section along the Y-direction, as shown in Fig. 10 and Fig. 11. The largest relative error norm of the displacement with FEMs (ANSYS) is 2.5%, the largest error norm of the mises-stress is 2.4%, but the largest relative error norm of the displacement employing the proposed method is 0.3%, and the largest error norm of the mises-stress is 0.28%. Obviously, the accuracy of the method presented in the paper is superior.

By the analysis of results following conclusions can be drawn: firstly, the proposed method has good accuracy; secondly, the scale selected has a great influence on the computational accuracy of the method presented. In order to further analyze the correctness and precision of the method, under the condition of selecting the same scale parameter, we show the relative error norm of the displacement and stress with Gauss weight function, and compare them with the presented method.

Table 2 is shown as the relative error norm with the proposed method under various scales, and it is described with the error curve as Fig. 12. From Table 2 and Fig. 12, we can get conclusions that computation accuracy is affected by the scale parameter. When 3-order B-spline wavelet function is used as a weight function, the results are better than Gauss weight function as weight

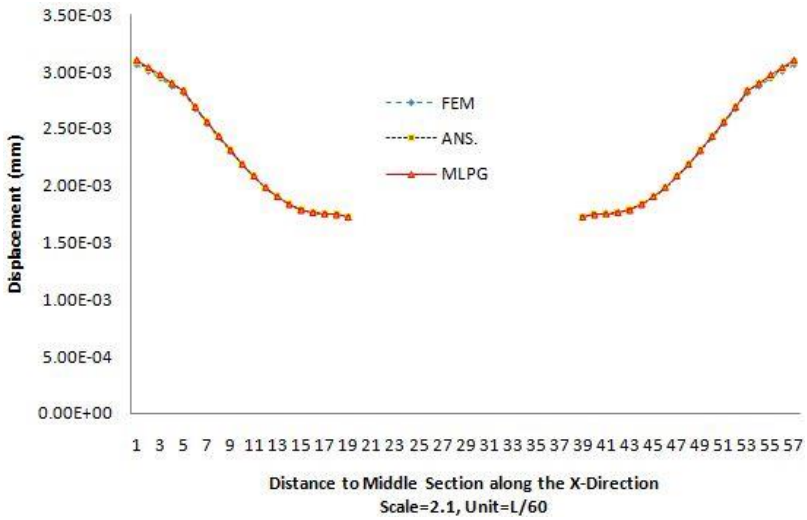


Fig. 11 Total deformation of the middle section along the *X*-direction

Table 2 The relative error norm with 3-order B-spline wavelet and Gauss weight function

| Scale | 2 | 2.1 | 2.5 | 2.8 | 3 | 3.5 | 4 |
|---|---|---|---|---|---|---|---|
| $L_u$-B | 10.6184 | 1.8542 | 7.9014 | 16.4551 | 4.334 | 7.5362 | 3.3685 |
| $L_\sigma$-B | 11.1394 | 3.5209 | 8.6167 | 17.0283 | 4.7365 | 8.0348 | 3.8175 |
| $L_u$-G | 15.6284 | 9.8024 | 7.9167 | 4.3211 | 5.6237 | 7.2018 | 10.1034 |
| $L_\sigma$-G | 15.3478 | 9.1273 | 8.8766 | 4.0325 | 5.7892 | 8.0121 | 11.2089 |

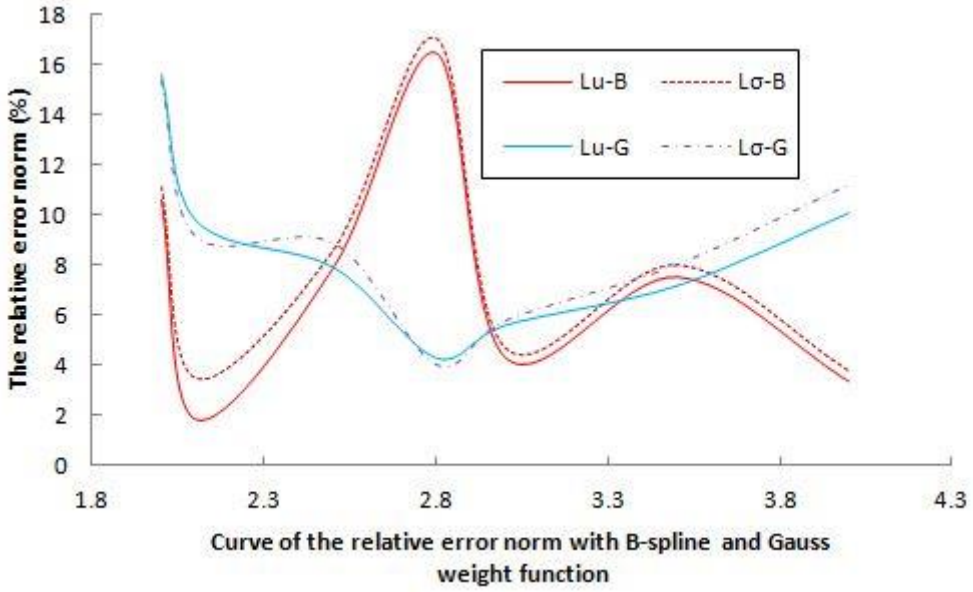


Fig. 12 The relative error norm with 3-order B-spline wavelet and Gauss weight function

function. In addition, the proposed method can achieve a good accuracy in the case of small support domain, namely, while *Scale*=2.1, it can achieve a higher fitting.

## 5. Conclusions

The paper presents a mesh-free method of the ship structures based on meshless local MLPG method. Based on meshless local Petrov-Galerkin, employs m-order B-Spline function as the wavelet basis function to construct the approximating function of the membrane structures. The general applicability of the presented approach has been demonstrated through the two application examples, namely the plate beam structure and the structure with circular opening. It is shown to be accurately predicated. The results show good agreement with FEMs (ANSYS) and verify the presented method is valid. The paper calculated the relative error norm of the displacement and stress with Gauss weight function, and then compared them with the proposed method. The results are more satisfying than Gauss weight function. Nevertheless, the proposed method can achieve a good accuracy in the case of small support domain. The proposed approach provides significant computational benefits and feasible method to deal with the analysis of the membrance structures.

## Acknowledgments

This work is supported by Guangdong Natural Science Foundation under Project: Research on Adaptive Coupling Finite element and Meshless Method of Ship Structures, and is also supported by China Postdoctoral Science Foundation: Research on Mesh-free Analysis Method of Fluid-Solid Interaction about the Vortex-Induced Vibration of Deep-water Risers

## References

Cui, W.C., Cai, X.G. and Leng, J.X. (1998), "A State-of-the-Art review for the fatigue strength assessment of ship structures", *J. Ship Mech.*, **2**(4), 63-81.

Na, S.S. and Karr, D.G. (2013), "An efficient stiffness method for the optimum design of ship structures based on common structural rules", *Ship. Offshore Struct.*, **8**(1), 29-44.

Norwood, M.N. and Dow, R.S. (2013), "Dynamic analysis of ship structures", *Ship. Offshore Struct.*, **8**(3-4), 270-88.

Senjanovic, I., Hadzic, N. and Bigot F. (2013), "Finite element formulation of different restoring stiffness issues in the ship hydroelastic analysis and their influence on response", *Ocean Eng.*, **59**, 198-213.

Tezduyar, T. (2003), "Computation of moving boundaries and interfaces and stabilization parameters", *Int. J. Numer. Meth. Fluid.*, **43**, 555-575.

Belytschko, T., Krongauz, Y., Organ, D., Fleming, M. and Krysl, P. (1996), "Meshless methods: An overview and recent developments", *Comput. Meth. Appl. Mech. Eng.*, **139**, 3-47.

Liu, W.K., Hao, S., Belytschko, T., Li, S. and Chang, C.T. (1999), "Multiple scale meshless methods for damage fracture and localization", *Comput. Mater. Sci.*, **16**, 197-206.

Atluri, S.N. and Shen, S. (2005), "The basis of meshless domain discretization: the meshless local Petrov-Galerkin (MLPG) method", *Adv. Comput. Math.*, **23**, 73-93.

Oden, J.T., Duarte, C.A. and Zienkiewicz, O.C. (1998), "A new could-based hp finite element method", *Int. J. Numer. Meth. Eng.*, **50**, 160-170.

Liu, G.R. and Gu, Y.T. (2000), "Meshless local Petrov-Galerkin method in combination with finite element and boundary element approaches", *Comput. Mech.*, **26**, 536-646.

He, P.X., Li, Z.X. and Wu, C.C. (2006), "Coupled finite element-element-free Galerkin method for dynamic fracture", *Chin. J. Appl. Mech.*, **23**(2), 195-198.

Duan, N., Wang, W.S., Yu, Y.Q., Huang, H. and Xu, X.P. (2013), "Dynamic simulation of single grain cutting of glass by coupling FEM and SPH", *Chin. Mech. Eng.*, **24**(20), 2716-2721.

Johnson, G.R., Stryk, R.A., Beissel, S.R. and Holmquist, T.J. (2002), "An algorithm to automatically convert distorted finite element into meshless particles during dynamic deformation", *Int. J. Impact Eng.*, **27**, 997-1013.

Liu, G.R. (2003), *Meshfree Methods Moving Beyond the Finite Element Method*, CRC Press.

Atluri, S.N. and Zhu T. (1998), "A new meshless local Petrov-Galerkin (MLPG) approach in computational mechanics", *Computat. Mech.*, **22**, 117-179.

Zienkiewicz, O.C. (1989), *The Finite Element Method*, 4th Edition, McGraw-Hill, London.

Yang, Y.Y. and Li, J. (2005), "A study of weight function in elemen-t free Galerkin method", *J. Plast. Eng.*, **12**(4), 5-9.

Chen, J.P., Tang, W.Y. and Xu, M.P. (2015), "A mesh-free analysis of the Ship Structures Based on Daubechies Wavelet Basis theory", *J. Inform. Comput. Sci.*, **12**(5), 1675-1684.

Long, S.Y. and Hu, D. (2003), "A study on the weighted function of the moving square approximation in the local boundary integral equation method", *Acta Mechanica Sinica*, **16**(3), 276-282.

Mallat, S. (1989), "Multiresolution approximations and wavelet orthonormal bases of L2(r)", *Tran. Am. Math. Soc.*, **315**, 69-87.

Qin, R. (2012), *Spline Meshless Method*, Science Press, Beijing, China.

Cui, C.K. and Quak E. (1993), "Wavelets on a bounded interval", *Numer. Meth. Approx. Theor.*, **1993**(1), 53-57.

Chen, J.S., Pan, C., Wu, C.T. and Liu, W.K. (1996), "Reproducing Kernel Particle Methods for large deformation analysis of nonlinear structures", *Comput. Meth. Appl. Mech. Eng*, **139**, 195-229.